# A Long Look at NGC 3783 with the *XMM-Newton* Reflection Grating Spectrometers

Ehud Behar[1], Andrew P. Rasmussen[2], Alexander J. Blustin[3], Masao Sako[4,5], Steven M. Kahn[2], Jelle S. Kaastra[6], Graziella Branduardi-Raymont[3], Katrien C. Steenbrugge[6]

## ABSTRACT

A long 280 ks observation of the Seyfert 1 galaxy NGC 3783 with *XMM-Newton* is reported. We focus on the oxygen line complex between 17 and 24 Å as measured with the RGS spectrometers. Accurate absorption column densities and emission line fluxes are obtained. We explore several options for the geometry and physical form of the emitting and absorbing gas. The lack of change in ionization in the absorber despite an increase in continuum flux during the observation restricts the high-ionization (O-K) and the low-ionization (Fe-M) gas to distances of at least 0.5 pc and 2.8 pc, respectively, away from the central source. Given the P-Cygni type profiles in the resonance spectral lines and the similar velocity widths, column densities, and ionization structure inferred separately from the emission and absorption lines, it is tempting to relate the X-ray narrow-line emitting plasma with the X-ray absorbing gas. Under this assumption, the scenario of dense clumped clouds can be ruled out. Conversely, extended ionization cones ($r \gtrsim 10$ pc) are consistent with the observation independent of this assumption. These findings are in stark contrast with the picture of numerous clumpy ($n_e \gtrsim 10^9$ cm$^{-3}$) clouds drawn recently from UV spectra, but it is consistent with the extended X-ray emission cones observed directly in Seyfert 2 galaxies.

*Subject headings:* Galaxies: Active, Individual (NGC 3783) — Techniques: Spectroscopic — X-Rays: Galaxies

[1]Physics Department, Technion, Haifa 32000, Israel; behar@physics.technion.ac.il

[2]Columbia Astrophysics Laboratory, Columbia University, 550 West 120th Street, New York, NY 10027

[3]MSSL, University College London, Holmbury St. Mary, Dorking, Surrey RH5 6NT, UK

[4]Theoretical Astrophysics and Space Radiation Laboratory, California Institute of Technology, MC 130-33, Pasadena, CA 91125

[5]*Chandra* fellow

[6]Space Research Organization of the Netherlands, Sorbonnelaan 2, 3548 CA, Utrecht, The Netherlands

## 1. Introduction

As a bright, nearby Seyfert 1 galaxy [z = 0.00976, de Vaucouleurs et al. (1991)], NGC 3783 is one of the best studied Active Galactic Nuclei (AGN). In the X-rays, observations with *ROSAT* (Turner et al. 1993) and *ASCA* (George et al. 1998) revealed a highly-ionized absorber, but lacked the spectral resolution required for kinematic measurements. Lately, the rich absorption line spectrum of NGC 3783 has been readily measured with the grating spectrometers on board the X-ray observatories *Chandra* (Kaspi et al. 2000, 2001, 2002) and *XMM-Newton* (Blustin et al. 2002), telling us that the highly-ionized gas is outflowing at velocities of a few 100 km $s^{-1}$. These spectra of NGC 3783 feature numerous absorption lines by K-shell ions of C, N, O, Ne, Mg, Si, and S, as well as by L-shell ions of Fe. Many inner-shell absorption lines formed by lower ionization states are also found in NGC 3783 (Behar & Netzer 2002) indicating a broad range of ionization.

Kaspi et al. (2002) used the high resolving power ($\lambda/\Delta\lambda$ up to 1000) of the *Chandra* High Energy Transmission Grating Spectrometer (HETGS which covers the 1.6 - 23.4 Å wavelength range) to determine the mean outflow velocity of $-590 \pm 150$ km $s^{-1}$ and a mean FWHM of $820 \pm 280$ km $s^{-1}$ for the absorber in NGC 3783. The unprecedented small errors are due to an integrated observing time of 900 ks. Both velocities are consistent with a blend of known UV absorption systems. Blustin et al. (2002) employed a short 40 ks observation of NGC 3783 with the Reflection Grating Spectrometers (RGS, $\lambda/\Delta\lambda$ up to 400) on board *XMM-Newton* to construct a plasma model with two ionization phases in the X-ray absorber that reproduced the RGS spectrum between 6 and 38 Å quite well. However, as was also pointed out by Kaspi et al. (2001), the wide range of observed charge states is indicative of a broad distribution of ionization within each phase. Despite the extensive X-ray measurements, the location, form, and energetic significance of the outflow in NGC 3783 have remained much of a mystery.

The connection of the X-ray absorber to AGN constituents observed in other wavebands is a long standing puzzle. The broad-line region (BLR) in NGC 3783 is inferred from the optical time lag measurements of Onken & Peterson (2002) to cover a range of distances from approximately $10^{15}$ to $10^{16}$ cm (not along the line of sight). Combining X-ray and UV observations, Shields & Hamann (1997) favor the interpretation by which the UV and X-ray absorbers constitute a single medium. Their analysis implies an upper limit of about 30 pc for the separation between the nucleus and the absorbing plasma. Recently, four velocity components have been resolved by Gabel et al. (2003) in the UV absorption spectrum of NGC 3783. Interpreting absorption of C III at 1175 Å as arising from a metastable level, Gabel et al. (2003) estimate the electron density in the high-velocity component to be $n_e \cong 10^9$ $cm^{-3}$ and, hence, the absorber to be located at a distance $r \leq 8 \times 10^{17}$ cm away from

the central source and with a typical size of $\Delta r \cong 10^{10}$ cm, i.e., numerous highly-clumped cloudlets. Conversely, a narrow O VI *emission* line component with a centroid velocity of 0 km s$^{-1}$ was estimated by Gabel et al. (2003) to originate about 40 pc away from the nucleus.

In December 2001, *XMM-Newton* observed NGC 3783 for 280 ks. The high effective area of the RGS makes this data set comparable in statistical quality to that obtained in 900 ks with the HETGS in the respective wavebands. In this paper, we present the RGS spectrum from this long observation. The main goal is to further characterize the X-ray absorbing and emitting gas and particularly to constrain its geometry and physical conditions.

## 2. The Data

### 2.1. Data Reduction

NGC 3783 was observed by *XMM-Newton* for a total of 280 ks from December 17 - 21 as part of the RGS guaranteed time program. The data obtained with the EPIC X-ray cameras and with the Optical Monitor (OM) will be discussed elsewhere (Blustin et al., in preparation). Here we focus on the RGS spectrum. The RGS data were processed using custom software developed at Columbia University, which operates on the observation data files (ODF). This software is similar in origin and in function to the RGS branch of the science analysis system (SAS), but is more flexible and includes recent calibration of the instrumental O-edge region based on accumulated data from long observations of Mrk 421 (Rasmussen, Paerels, & Kahn 2003). It corrects for the effect of aspect drift on the dispersion angles and includes background subtraction using off-target CCD regions.

### 2.2. Short Time Variability

The RGS light curves are shown in Fig. 1. It is evident that the soft X-ray flux varies fitfully and by as much as a factor of 2 on time scales of hours. The light curves obtained with the EPIC cameras, which are more sensitive to hard X-rays, show very similar behavior. The UV light curve obtained with the Optical Monitor (OM) resembles the curve in Fig. 1, only it is somewhat smoother (Blustin et al., in preparation). Observed variations in the ionization state of the absorber due to changes in the continuum flux could potentially shed light on the location of the absorber through ionization and recombination times. With that goal in mind, we divide the 280 ks observation into four temporal segments, seeking variations in the absorption spectrum.

The four segments are labeled in Fig. 1 as the "low", "rise", "high", and "peak" phases. The spectra obtained for each segment separately are presented in Fig. 2. Each segment by itself suffers from limited statistics. Consequently, disparities in narrow features such as emission or absorption lines, which have limited counts in a few bins, are very difficult to detect unambiguously. On the other hand, it is clearly seen that the broad absorption features in the spectrum, such as the Fe M-shell 2p - 3d unresolved transition array (UTA) between 16 and 17 Å and the O VII and O VIII photoelectric bound-free K-edges (just noticeable at 14.2 & 16.8 Å) do not vary significantly from one time segment to the other. Indeed, calculated ratios of spectra among the various time segments show mostly noise around the flat ratio of the continua to within the data errors, i.e., ∼10%. For example, the ratio of the "high" and "low" segments is plotted in Fig. 3. The plot is rather noisy, but no clear bound-free edge features are observed. The only statistically significant deviations from the mean in Fig. 3 are well localized around strong emission/absorption lines (e.g., Ne IX at 13.48 Å). Since emission lines are not expected to disappear in the ratio plot and since ratios at deep absorption troughs are unreliable, we interpret the lack of bound-free features as evidence for no detectable variation in absorption.

The position and shape of the Fe-M 2p-3d UTA are expected to be particularly sensitive to the ionizing flux as several M-shell charge states of the same element are observed at the same time. During the present observation, the ionizing flux overall increased gradually by almost a factor of 2 (Fig. 1). An average increase of about 50% occurs from the "low" state to the "high" state. Such an increase in the ionization parameter $\xi$ [$\xi = L/(n_e r^2)$, where $L$ is the ionizing luminosity] would have shifted the UTA towards shorter wavelengths by about 0.4 Å, if the gas had reached a new equilibrium state (c.f., Fig. 4 in Behar, Sako, & Kahn 2001). Such a shift would have been surely detectable with the RGS. Carefully examining Fig. 3, it is possible to visualize a slight, statistically insignificant, shift in the UTA around 16 Å. However, this is exactly where the O VIII Ly$\beta$ line falls and in any event the effect is smaller than would be expected from new equilibrium conditions. Together with the lack of edge features in Fig. 3, this makes for strong evidence that the ionization state in the absorber does not have ample time to reach a new equilibrium state and, thus, it is hardly affected by the rapidly varying continuum.

Since the ionization time depends directly on the absolute ionizing flux seen by the absorber (i.e., its distance from the source), we can use the lack of ionization despite the increase in flux to place a lower bound to the separation between the source and the absorber. For a detailed discussion of ionization in winds, see Krolik & Kriss (1995). We take the average power-law ionizing flux density $F_E = A(E/E_0)^{-\Gamma}$ with $E_0 = 1$ keV and $\Gamma \cong 1.7$ (determined for NGC 3783 by Kaspi et al. 2001; Blustin et al. 2002, and here). The normalization factor $A$ scales with $r^{-2}$ and reaches its observed value of about 0.015

photons $s^{-1}$ $cm^{-2}$ $keV^{-1}$ at the telescope at a distance of 41.8 Mpc (assuming $H_0 = 70$ km $s^{-1}$ $Mpc^{-1}$). To first order and as an upper limit, the equilibration time is the reciprocal of the photoionization (PI) rate $\int F_E \sigma^{PI}(E) dE$, where $\sigma^{PI}(E)$ is the PI cross section. For O VII, we get a time of 4.6 $r^2_{[pc]}$ days, where $r_{[pc]}$ is the distance of the absorber from the source in parsecs. The unnoticeable change in ionization observed over more than a day following the rise of the continuum implies that the O VII absorber is at least 0.46 pc away from the source. Extrapolating the power law continuum down to the ionization energy of Fe IX ($\cong$ 0.23 keV), which is dominant in the Fe-M UTA (at about 16.6 Å), but also representative of the other M-shell ions, we get an even shorter ionization time of about 0.13 $r^2_{[pc]}$ days. Consequently, the Fe IX absorber must be at least 2.8 pc away from the source to not be affected. Although only crude lower limits, these estimates already clearly exclude the BLR, which is approximately 0.003 pc away from the source (Onken & Peterson 2002). For comparison with previous estimates, Appenzeller & Wagner (1991) place emission by highly-ionized species (e.g., Fe VII) just outside the BLR, while Shields & Hamann (1997) give an upper limit of 30 pc for the X-ray and UV gas.

Note that despite the fluctuations over time scales of days, the average X-ray flux in NGC 3783 has remained steady over the past few years (e.g., Markowitz et al. 2003). Under these conditions and at a distance $\gtrsim$ 0.5 pc, the ionization state of the absorber does not react to the short time-scale fluctuations, but instead it is governed entirely by the mean flux. Indeed, Kaspi et al. (2001) point out that the shape of the X-ray absorption spectrum of NGC 3783 is unchanged since 1996 when it was measured with *ASCA*, although the continuum level has clearly varied during that period. A study of spectral variability on intermediate time scales of a few months using fractions of the 900 ks HETGS observation is bound to shed new light on the behavior of NGC 3783 in time (Netzer et al., in preparation).

### 2.3. Time Integrated Spectrum

The fact that the absorption in the spectrum does not vary significantly during the course of our observation justifies the treatment of the 280 ks time integrated spectrum as a whole for studying the absorption. Furthermore, when we compare the present average spectrum with earlier observations (Kaspi et al. 2001, 2002; Blustin et al. 2002), we still find no significant discrepancies. Consequently, for the most part the best-fit model proposed by Blustin et al. (2002) describes the current spectrum rather well. This is demonstrated in Fig. 4 where the slab model from Blustin et al. (2002) is compared with the current 280 ks spectrum. No adjustment whatsoever has been applied to the model, including no renormalization. Noticeable discrepancies between data and model occur in the details around

the O K$\alpha$ region between 14 and 24 Å. These could not have been modeled properly with the first 40 ks exposure due to lack of counts in the narrow lines present in this range.

In this work, we focus on the O I - O VIII complex in the wavelength range 17.3 - 24.7 Å. The goal is to measure individual emission and absorption line fluxes. Due to considerable blending, a simultaneous fit of many spectral features is required. We fit the spectrum locally with a power-law plus an ensemble of individual-ion absorption models and a few (unabsorbed) emission lines. Subsequently, galactic absorption ($N_H = 8.7{\times}10^{20}$ cm$^{-2}$) is applied to the entire spectrum. The models are based on atomic data calculated with HULLAC (Bar-Shalom, Klapisch, & Oreg 2001) and include all of the inner-shell atomic transitions and their autoionization widths for all ions and elements that appear in the spectrum. A similar method has been successfully applied to several previous AGN spectra (e.g., Sako et al. 2001; Kaastra et al. 2002; Blustin et al. 2002).

### *2.3.1. Absorption*

Out of four velocity components resolved in the UV (e.g., for O VI), of which two are marginally resolved with HETGS in lines of O VII and O VIII (Kaspi et al. 2002), the RGS reveals only one blended trough. Indeed, the blueshifts measured here ($\cong -600$ km s$^{-1}$) are consistent with the mean velocity of the two dominant (& slowest) components in the UV and are in agreement with the velocity measured with HETGS. Thus, in the model, we use only one velocity component for each ion. We fit for the turbulent velocity width and obtain $v_{turb} = 170$ km s$^{-1}$ (i.e., $\sigma_v = 120$ km s$^{-1}$, FWHM = 280 km s$^{-1}$). This width is very close to the value of 150 km s$^{-1}$ used by Kaspi et al. (2000). Both here and in Kaspi et al. (2000), this velocity width was used because it enables the fitting of entire series of lines with a single kinematic component. However, it should be clear that the actual absorption troughs comprise more than one intrinsic velocity component and are broader. In fact, Kaspi et al. (2001, 2002) measured directly $v_{turb} = 500 \pm 170$ km s$^{-1}$. In fitting the spectrum, we assume a covering factor of unity, which is an approximation for the value of 0.8 obtained by Gabel et al. (2003), who fit for the covering factor of the X-ray observed components in the UV spectra. The present velocity-blended spectrum is not sensitive to this difference. Emission lines are modeled by Gaussians. None of these approximations hamper the good estimates we get for the total column density in each ion and for the total flux in each emission line, which are the physical quantities of interest here.

The best-fit spectral model for the O region is given in Figs. 5 and 6, highlighting respectively the K$\alpha$ and K$\beta$ (and higher) transition regions. The good fit, including that for the high-order lines of the He-like series below 19 Å, is apparent in the figures. Absorption

by all charge states from O VIII down to O IV is clearly detected. It is obvious from the figures that it is crucial to fit all charge states simultaneously, including both absorption and emission, in order to obtain the correct physical measurements. The various ions are found outflowing at (indistinguishable) centroid velocities of $-470$ - $-800$ km s$^{-1}$ with respect to the systemic velocity of NGC 3783. The fitted parameters for each of these ions are given in Table 1.

Evidently, the broad range of charge states observed along the line of sight is ubiquitous to Seyfert outflows (Sako et al. 2001; Behar & Netzer 2002; Blustin et al. 2003; Steenbrugge et al. 2003). It is also observed in Seyfert 2 galaxies (Kinkhabwala et al. 2002). If all charge states are present at similar distances from the central source, as observed directly in Seyfert 2's, it implies a strong density gradient of 3-4 orders of magnitude (e.g., for O IV to O VIII) over relatively short distances. In turn, comparable column densities together with a strong density gradient would imply that the highly-ionized gas occupies a much larger volume than the less-ionized gas. This picture is consistent with a wind that emanates from a dense object (e.g., accretion disk or bloated stars). It then accelerates, expands and becomes hotter and more ionized. Pressure equilibrium also favors the hotter gas being more tenuous and therefore more extended.

In addition to the high charge states, weak absorption by O I and O II may also take place in (the rest frame of) NGC 3783 as indicated in Fig. 5. However, blending with other ions hampers an unambiguous detection. The O I K$\alpha$ line in NGC 3783 overlaps with the strongest absorption lines of Ar XVI at 23.529 Å (Lepson et al. 2003). The O II K$\alpha$ line in NGC 3783 can not be resolved from the local galactic K$\alpha$ line in our own galaxy. O III is not detected. Nevertheless, since we simultaneously fit many lines from each ion, we are able to overcome the problem of blending to some extent and to provide upper limits to the ionic column densities. Of course, these constrains are not as tight as those provided by UV measurements for the same ions, when those are available (Kraemer, Crenshaw, & Gabel 2001).

The errors on the outflow velocities are relatively large due to the wavelength channel widths of the RGS. Estimating the uncertainty to be bound by 3 channels implies an error range of $\pm$ 16.5 mÅ corresponding at 22 Å to $\pm$ 230 km s$^{-1}$ as quoted in Table 1. The best-fit column densities are also given in Table 1. The column densities of O VII and O VIII are constrained most tightly by their detected photoelectric edges. An additional constraint is imposed by fitting entire series of lines (see also Fig. 6). The values of (1.0 $\pm$ 0.3) and (4.0 $\pm$ 1.0) $\times$ 10$^{18}$ cm$^{-2}$ obtained for the column densities of O VII and O VIII, respectively, are in excellent agreement with the values of 1.1 and 4.3 $\times$ 10$^{18}$ cm$^{-2}$ obtained by Kaspi et al. (2002).

The O VI ion is of particular interest for the possible connection between the UV and X-ray absorbers. Inner-shell O VI absorption can be observed in the present spectrum although only marginally. We detect the K$\alpha$ line at a significance of about 2 sigma over a total of 4 wavelength channels, but the errors on the data points are still too large to see the line profile clearly (compare data with continuum model in Fig. 5). The feature at 19.33 Å can be associated with the O VI K$\beta$ line, although it is mostly due to O V K$\gamma$ (see Fig. 6). The derived column density of O V is much higher than that of O VI. This is due to the closed shell structure of O V and to the pervasively low fractional abundance of the Li-like species O VI ($< 0.25$, e.g. Kallman & Bautista 2001). To that end, O VI and Li-like ions in general are perhaps the least favorable vestige for probing the ionized outflow in AGN. The precise restframe wavelengths of the K$\alpha$ inner-shell transitions in O ions have yet to be measured in the laboratory and are still somewhat in debate (Behar & Kahn 2002). Here, we use wavelength values for O VI K$\alpha$ and K$\beta$ of 22.01 and 19.34 Å, respectively. With a fitted turbulent velocity of 170 km s$^{-1}$, we obtain only an upper limit to the O VI column density of $2.0 \times 10^{16}$ cm$^{-2}$. This is loosely consistent with Gabel et al. (2003), who find a lower limit of $0.63\times 10^{16}$ cm$^{-2}$ for the total O VI column density in the two corresponding UV components. We note that there was a hint to the K$\alpha$ line of O VI in the 900 ks HETGS spectrum (Kaspi et al. 2002), but there, the lower statistical quality did not allow for a definite identification.

The present high-quality spectrum reveals an absorption feature at 21.64 Å (21.43 Å in Fig. 5 at the rest frame of NGC 3783). We identify it tentatively as absorption by O VII in the intergalactic medium (IGM). Given this interpretation, the gas would be at a redshift of $z = 0.0018 \pm 0.0008$. The absorption parameters deduced for this line are given in Table 1. Another possible identification for this line could be Ca XVI (21.49 Å in the rest frame) in the outflow of NGC 3783, but lines by neighboring charge states of Ca are not as obvious in the spectrum, which casts doubt on the identification of Ca. Since this feature may not be related to NGC 3783, we defer a more careful analysis of it to a separate paper. There is a hint of this line in the 900 ks HETGS spectrum, but there it seems to be at 21.60 Å (as opposed to 21.43 Å), where local O VII would be expected. In any event, due to the lower statistical quality of the HETGS observation in this spectral band, Kaspi et al. (2002) conclude that it is insignificant.

### *2.3.2. Emission*

In addition to the numerous absorption lines, a few bright, narrow emission lines are present in the spectrum. In the O region of the spectrum, the brightest emission lines are

O VIII Ly$\alpha$ at $\sim$ 19 Å and the He$\alpha$ triplet of O VII at $\sim$ 22 Å (the resonance, intercombination, and forbidden lines - $r, i, \& f$). The radiative recombination continuum (RRC) of O VII is also detected, although its location at 16.8 Å in the midst of the Fe-M 2p - 3d UTA makes a precise determination of its flux rather difficult. In fact, it is much better resolved with HETGS (Fig. 6 in Kaspi et al. 2002). The weaker O VII and O VIII K$\beta$ as well as higher-order emission lines have been identified with HETGS (Kaspi et al. 2002), but here the lower spectral resolution impedes the measurement of their flux. The measurable O emission features are listed in Table 2. Fitting for a uniform velocity width for all emission lines, we obtain a turbulent velocity of $740 \pm 140$ km s$^{-1}$ (FWHM $1220 \pm 230$ km s$^{-1}$). Kaspi et al. (2002) measured a FWHM of $930 \pm 350$ km s$^{-1}$ for the most isolated O VII $f$-line. Previous optical measurements by Appenzeller & Östreicher (1988) of narrow, forbidden emission lines of highly-ionized species in NGC 3783 show a consistent linear increase in velocity width with ionization energy. The presently measured width of 1220 km s$^{-1}$ FWHM for O VII fits that trend perfectly (see their Fig. 13). For O VIII, we are not able to provide an independent measurement of the emission line width, because there are no O VIII non-absorbed (forbidden) lines in the spectrum.

As evident from Figs. 5 and 6, the emission/absorption model fits the data (including the intricate line profiles) remarkably well. This gives confidence in the individual (deblended) line fluxes obtained. All of the measured emission lines are slightly redshifted by about $300 \pm 230$ km s$^{-1}$. Owing to the large errors, this is still consistent with the mean shift of $130 \pm 290$ km s$^{-1}$ measured for the emission lines with HETGS (Kaspi et al. 2002). These redshifts together with the complex P-Cygni type profiles seen for the resonance lines are suggestive of a bipolar outflow as discussed in detail below. Also presented in Table 2 are the line fluxes measured with HETGS. The current values are in good agreement with the HETGS values. The largest discrepancies are found for the resonance lines, which have complicated P-Cygni type profiles [Ly$\alpha$ and He$\alpha(r)$]. This is due to the different methods used for measuring the line fluxes. For example, Kaspi et al. (2002) did not fit for overlapping absorption and did not require the widths of the three O VII lines to be uniform. Nonetheless, the general agreement between the two measurements implies no time variation as expected for the narrow line region (NLR).

## 3. Discussion

### 3.1. Relation Between the X-Ray Emitter and Absorber

To summarize the X-ray outflow kinematics in the rest frame of the AGN as manifested by the absorption and emission lines: The emission lines are redshifted by about

300 ± 230 km s$^{-1}$ and have FWHM of 1220 ± 230 km s$^{-1}$ (present work). The absorption lines are blueshifted by about −600 ± 150 km s$^{-1}$ and have a FWHM of 820 ± 280 km s$^{-1}$ (Kaspi et al. 2002). Although it is impossible to constrain the exact shape of the X-ray line profiles and in particular their broad wings, due to the crowded nature of this waveband and the overlapping emission and absorption, it is obvious that high-velocity gas (up to ∼1000 km s$^{-1}$) is both emitting and absorbing X-rays. For the resonance lines, P-Cygni type profiles are observed (Figs. 5 & 6). These line profiles are characteristic of a bipolar, non-collimated outflow in conjunction with absorption by the outflow along the line of sight. It is important to point out that we have only approximated these profiles by emission and (slightly offset) absorption lines, but the comparable velocity widths obtained for the absorption and emission lines already supports the biconical interpretation.

We wish to further compare the X-ray line emission and absorption in NGC 3783. In the context of Seyfert 2 galaxies, it has been shown that intensity ratios among the He-like emission lines can be used to decisively determine the column density through the emitting plasma (Behar et al. 2001; Kinkhabwala et al. 2002) even when the absorption spectrum is not available to us directly due to orientation & obscuration effects. The present emission line fluxes give ratios of $f/r = 1.5 \pm 0.3$ and $i/r = 0.5 \pm 0.2$. With the velocity width of 740 km s$^{-1}$, this $f/r$ value is obtained in our model at an O VII ionic column density of (1.1 ± 0.35) × 10$^{18}$ cm$^{-2}$. The $i/r$ ratio provides just a lower limit of 1.3 × 10$^{18}$ cm$^{-2}$. These ranges are both in good agreement with the ionic column density of (1.0 ± 0.3) × 10$^{18}$ cm$^{-2}$ measured directly from the absorption lines and edge of O VII.

Next, it would have been useful to compare the fractional ionic abundances derived from the emission lines with those derived from the absorption. However, direct comparison is not available since recombination-driven lines are due to the next ionized state (e.g., O IX for Ly$\alpha$). Hence, the O VII & O VIII emission line intensities reflect the $n_{OVIII}/n_{OIX}$ abundance ratio, while the absorption column densities reflect $n_{OVII}/n_{OVIII}$. Nevertheless, the comparable emission line fluxes and column densities of O VII and O VIII suggest that all highly-ionized states are fairly abundant in the emitting plasma, just as they are in the absorbing plasma. Moreover, it is possible to find an ionization parameter $\xi = 30$ erg s$^{-1}$ cm that reproduces just the right amount of O VII and O VIII emission and absorption, which we observe. Clearly, we are seeing a very broad distribution in $\xi$, but for simplicity, this single value can be used to describe the O VII & O VIII spectral features. In summary, the velocity widths, the column densities, and the fractional abundances all make it tempting to interpret the X-ray emitter and absorber as arising from the same gas.

### 3.2. Location and Geometry of the X-Ray Plasma

The measured emission line flux $F_{ji}$ (e.g., of an O ion) can be related to the volume ($V$) emission measure $EM$ as follows:

$$EM \equiv \int_V n_e n_H dV = \frac{4\pi d^2 F_{ji}}{f_{q+1} A_O P_{ji}} \tag{1}$$

The computed line power $P_{ji}$ is defined through the line emissivity $n_e n_q P_{ji}$ (i.e., number of line photons emitted in the plasma per unit time and per unit volume). Here, $n_q$ is the number density of ions with charge $q$. The line power takes into account all line-driving mechanisms and in particular recombination, radiative cascades, and photoexcitation. The fraction of ions with charge $q$ ($n_q/\Sigma n_{q'}$) is denoted by $f_q$. For recombination-driven emission lines such as the present ones, the most relevant fraction is $f_{q+1}$. In eq. (1), $A_O$ represents the oxygen elemental abundance relative to Hydrogen. The distance to the source $d$ is taken, for the case of NGC 3783, to be 41.8 Mpc. In a fully ionized cosmic plasma, we can also relate the electron density to the Hydrogen density by $n_e = 1.2\ n_H$. On the other hand, the column density $N_H$ can be written as follows:

$$N_H \equiv \int_{r_{min}}^{r_{max}} n_H dr = \frac{n_H}{n_e} \frac{L}{\xi} \left( \frac{1}{r_{min}} - \frac{1}{r_{max}} \right) \tag{2}$$

The measured ionic column densities $N_i$ are related to $N_H$ by $N_i = f_q A_O N_H$. The minimal and maximal distances for absorbing gas in the outflow are denoted by $r_{min}$ and $r_{max}$. To obtain the right hand side of eq. (2), we used $n_e = L/(\xi r^2)$.

We focus here on the O VII and O VIII spectral features as the tracers of the very highly-ionized gas simply because they exhibit the best measurable features in our spectrum. However, since Seyfert 2 observations show that all charge states co-exist and overlap in space along the outflow, we expect the present analysis of O ions to be applicable to the entire highly-ionized plasma. We choose an ionization parameter of $\xi = 30$ erg s$^{-1}$ cm, where ionization balance calculations give $n_{OVIII}/n_{OIX} \cong 1.7$ (in accord with the emission line ratio) and $n_{OVIII}/n_{OVII} \cong 4$ (in accord with the absorption column densities). This implies $f_q$ values of 0.14, 0.57, and 0.29, respectively for O VII, O VIII, & O IX. Again, a single value of $\xi$ is assumed in this section just for simplicity. The observed broad distribution in $\xi$ makes it clear that each ion exists mostly around its typical range of $\xi$.

Equations (1) & (2) can not be solved for the most general case and some approximations need to be made. In the following we explore the two extreme scenarios: $r_{max} \cong r_{min}$ and $r_{max} \gg r_{min}$.

### *3.2.1. Localized Scenario*

First, we explore the possibility of a well localized X-ray plasma, i.e., one in which the typical size $\Delta r = r_{max} - r_{min}$ is much smaller than the average distance $r$ from the ionizing source. In that case, the localization in $r$ immediately imposes a narrow distribution in $n_e$ (through $\xi$). Eqs. (1) and (2) can then be rewritten simply as: $EM = n_H n_e \Delta r^3$ and $N_H = (n_H/n_e)(L/\xi)(\Delta r/r^2)$. Even now, these equations can not yet be solved separately. However, if one identifies the emitter with the absorber, both equations can be solved simultaneously. Indeed, by using eqs. (1), (2), and the definition of $\xi$ to solve for $r$, $\Delta r$, and $n_e$ one would expect to obtain a rough idea of these quantities. However, using the present measurements for the O VII forbidden line and for the O VIII Ly$\alpha$ line, in both cases, we obtain values of $r \cong \Delta r \cong 10$ pc. This suggests that the confined geometry ($\Delta r \ll r$) is inadequate for describing the highly-ionized outflow of NGC 3783, at least as long as the line emission and absorption are due to the same outflow constituent. All of the measured and derived quantities are summarized in Table 3.

### *3.2.2. Ionization Cone Scenario*

Inspired by the *Chandra* X-ray images of Seyfert 2 galaxies (Sako et al. 2000; Young, Wilson, & Shopbell 2001; Brinkman et al. 2002; Ogle et al. 2003), we propose an alternative geometry of two ionization cones with an opening solid angle $\Omega$. In NGC 1068, AGN driven X-rays are detected as far as 500 kpc away from the nucleus (Brinkman et al. 2002). Furthermore, Young et al. (2001) & Ogle et al. (2003) show that the X-ray NLR in NGC 1068 overlaps on the plane of the sky with the optical NLR. Extended ionization cones in Seyfert 1's, only oriented along the line of sight, would substantiate the unified theory of AGN (Antonucci & Miller 1985) in the X-ray regime. Unfortunately, it is impossible to distinguish between clumpy clouds and ionization cones in NGC 3783 by means of X-ray imaging, as even the best angular resolution available with *Chandra* ($0''.5$) corresponds to 100 pc at the distance of NGC 3783. Therefore, we have to make use of the spectrum.

In the ionization cones scenario, the plasma covers a large range of distances (and densities) and it is necessary to revert to the integral forms of $EM$ and $N_H$ in eqs. (1) and (2) with $dV = 2\Omega r^2 dr$. Note that even within the framework of the extended geometry and even when $r_{max} \gg r_{min}$, for a given $\xi$ most of the absorption occurs close to $r_{min}$, while the actual size of the cones (i.e., $r_{max}$) can not be well constrained by the observation. Indeed, eqs. (1) and (2) can now be rewritten as:

$$r_{min} \cong (r_{min}^{-1} - r_{max}^{-1})^{-1} = \frac{n_H}{n_e} \frac{L}{\xi N_H} \tag{3}$$

and

$$\Omega = \frac{1}{2} \frac{EM}{N_H} \frac{\xi}{L} \tag{4}$$

In this scenario, since eq. (3) is attained from the column density alone without the emission measure, the result for $r_{min}$ is independent of the emission. Thus, it is independent of the assumption that the X-ray emitter and absorber represent the same plasma. Eqs. (3) & (4) demonstrate the dependence of the derived values on the assumption for $\xi$. Thus, if O VII actually forms at $\xi$-values somewhat lower than we assume (30 erg s$^{-1}$ cm), we would be slightly underestimating $r_{min}$ and overestimating $\Omega$, and vice versa. We stress that the focus on a certain ion or on a specific value of $\xi$ constitutes a complementary and totally consistent approach with the observation of a broad range of charge states. Again, analogous to the Seyfert 2 case, each charge state could be present throughout the cone, only at different densities, while at the same time different charge states are co-located thanks to the steep density gradients at each point in the cone. The X-ray observation simply traces O VII and O VIII wherever they are along the cone.

We now substitute the measured values into eqs. (3) & (4) using the data for the O VII forbidden line and for the O VIII Ly$\alpha$ line. These values as well as the results for $r_{min}$ and for $\Omega$ are summarized in Table 3. The electron density is again $n_e = L/(\xi r^2)$, but here it decreases rapidly ($\propto r^{-2}$) along the cone. In Table 3 we give the maximal $n_e$ value attained at $r_{min}$. It can be seen that the results for both O VII and for O VIII suggest consistently that the X-ray emitter/absorber lies at $r_{min} \cong 10$ pc. The maximal densities are of the order of 600 cm$^{-3}$. These results are not very different from those obtained by Shields & Hamann (1997), who do not assume a cone geometry, but give values of $n_e \gtrsim 50$ cm$^{-3}$ and $r_{min} \lesssim 30$ pc.

The typical opening angle $\Omega/2\pi$ we get for each of the two cones is about 15 - 25 %, fully consistent with the fraction of Seyfert galaxies that show a highly-ionized absorbing outflow (∼50% of the Seyfert 1's). The presently proposed geometry with the high $r_{min}$ and $\Omega$ values makes for a large scale outflow that from our perspective would entirely blanket the central AGN region including the BLR, provided that the ionization cone is uniformly filled. Since Gabel et al. (2003) find that at some radial velocities the BLR is only partially covered by the UV outflow, identifying the UV absorber with the extended X-ray ionization cone would require that some of the BLR be observed directly, i.e., through (velocity-specific)

holes in the cone. We note that Steenbrugge et al. (2003) estimate for NGC 5548 much smaller opening angles, $\Omega/2\pi < 0.5\%$. However, that result was obtained by assuming a mass loss rate that is equal to the mass accretion rate (with a luminosity efficiency of 5%). If this assumption is relaxed, extended ionization cones may be applicable for NGC 5548 as well. Indeed, the high values for $\Omega$ in NGC 3783 imply that the outflow mass loss rate exceed the accretion rate as discussed in the following section.

### *3.2.3. Mass Estimates*

By integrating the mass density $\mu n_H m_H$ (where $\mu = 1.3$ is the average atomic weight for a solar-abundance plasma) over the ionization cone (or clouds), it is possible to estimate the total mass $M$ and similarly the mass loss rate $\dot{M}$ in the outflow. These quantities are listed in Table 3 for both the localized and ionization cone models. In the ionization cone model, the total mass depends on $r_{max} - r_{min}$, which is not well constrained by the observation. Therefore, the mass in Table 3 is normalized to $r_{max} \cong r_{max} - r_{min}$. Taking an outflow velocity of $-600$ km s$^{-1}$, we obtain a total mass loss rate of up to a few solar masses per year. We compare this with an estimate of the mass accretion rate. With a bolometric luminosity of $4.5{\times}10^{44}$ erg s$^{-1}$ (Markowitz et al. 2003) and a gravitation-to-light conversion efficiency of $L_{bol}/(\dot{M}_{acc}c^2) = 5\%$, NGC 3783 would be accreting about 0.2 solar masses per year. If all these numbers are correct, then NGC 3783 is accreting only about 10% of the mass it is ejecting. Although this is a surprisingly low accretion efficiency, we are not aware of any hard evidence against it. Furthermore, ultra-high velocity outflows ($\sim$0.1c) have been discovered recently in several AGN. It has been postulated that the high mass loss rate observed in these sources is due to their high accretion rate $L_{bol}/L_{Eddington}$ (Pounds et al. 2003). Narrow line Seyfert 1's such as NGC 3783 could be the low-mass facet of this phenomenon.

It is worth stressing that the errors given in Table 3 reflect only those due to the presently measured $N_i$ & $F_{ji}$ values. Indeed, the present mass estimates should be treated with more caution as the X-ray outflow of NGC 3783 is undoubtedly more complex than a simple, continuous cone, which was assumed here. Nonetheless, these estimates are good enough to rule out radically different scenarios, such as the highly-localized one. Most likely, the true picture for NGC 3783 is somewhat less extreme than $r_{max} \gg r_{min}$ and therefore $r_{min}$ could be somewhat less than 10 pc, but certainly not much less, given the timing constrains obtained in Sec. 2.2 of $r_{min} \geq 0.5$ pc for O-K and $r_{min} \geq 2.8$ pc for Fe-M.

### *3.2.4. Comparison With Other Observations*

The extended ionization cones stand in contrast with interpretations of two other Seyfert 1 galaxies. Netzer et al. (2002), based on observed recombination times, place the ionized absorber in NGC 3516 about 0.2 pc away from the nucleus. Kriss et al. (2003) and Blustin et al. (2003) even suggest that part of the ionized absorber in NGC 7469 is closer to the nucleus than the BLR. In both of these cases, the observers find that the UV and X-ray absorbers are connected. More importantly, the present results are in stark contrast with the parameters derived by Gabel et al. (2003) for NGC 3783 based on UV absorption, which according to those authors occurs at sub-parsec distances in tiny clouds the size of $\Delta r \cong 10^{10}$ cm. At the heart of the argument of Gabel et al. (2003) lies the absorption by the C III multiplet at 1175 Å detected in the high-velocity UV component (-1300 km s$^{-1}$). Following Bromage et al. (1985), Gabel et al. (2003) take this feature as evidence for high-density gas ($\gtrsim 10^9$ cm$^{-3}$) in this component, which inevitably restricts it to clumps very close to the source. We wish to point out that the 2s2p triplet complex from which those C III lines are absorbed, can in fact be populated at lower densities. Only one fine-structure level in the triplet requires high densities (see, e.g., Fig. 1 in Bhatia & Kastner 1993), but absorption from the other two levels of the triplet may be possible at low densities and might be producing the C III lines at 1175 Å observed by Gabel et al. (2003).

On the other hand, it may also be possible that dense clouds reside at the base of the ionization cone where the outflow is clumpy, less ionized, and thus absorbs UV light. Further out in the outflow, perhaps, the ejecta evaporate, become much more tenuous and consequently more highly-ionized. These more extended parts of the outflow might then constitute the X-ray absorbing/emitting gas. However, following Kaspi et al. (2002) and Gabel et al. (2003), we note that the very similar velocity structure in the X-ray and UV absorption systems strongly suggests that the two coincide and most likely are two different manifestations of the same outflow. Finally, based on UV variability and recombination times, Shields & Hamann (1997) also arrive at the conclusion that the X-ray and UV absorbers are more than 10 pc away from the ionizing source.

A paramount difference between the UV-derived and X-ray-derived parameters of the outflow lies in the corresponding $M$ and $\dot{M}$ values. In the Gabel et al. (2003) picture, the calculated $M$ and $\dot{M}$ values are more than 10 orders of magnitude smaller than the values derived here from the X-ray measurement (see Table 3). According to the UV interpretation, the outflow carries insignificant mass and energy out of the AGN system, while according to the present X-ray analysis, the outflow must play a major role in the mass and energy budgets of the AGN.

## 4. Conclusions

The present 280 ks observation of NGC 3783 leads to a few interesting conclusions, which can be summarized as follows:

1. Despite the continuum increasing by up to a factor of 2 during the 280 ks observation, no significant effect on the absorption structure has been detected. The fact that the absorbing plasma did not respond to the increase in flux within, say, 1 day places it at least 0.5 pc (O-K) to 2.8 pc (Fe-M) away from the continuum source, regardless of its geometry or physical situation (e.g., density).

2. The interpretation of the X-ray line absorbing and emitting plasma being closely connected, or actually being manifestations of the same outflow, is very tempting given the P-Cygni type profiles as well as the similar velocity widths, inferred column densities, and ionization distributions.

3. Assuming that the two components are connected rules out the localized geometry ($\Delta r \ll r$ and $n_e \cong 10^9$ cm$^{-3}$) for the X-ray plasma. This geometry was suggested by Gabel et al. (2003) for the UV absorbing outflow.

4. Instead, we propose diffuse gas in the form of ionization cones. These cones may not be closer than about 10 pc from the ionizing source and must therefore have much lower densities (a few 100 cm$^{-3}$ and decreasing with distance). In this case, we find that the mass loss rate in the outflow is significant, of the order of a solar mass per year.

5. The conflict with the clumpy cloudlet description of Gabel et al. (2003) could possibly be due to erroneous use of the C III multiplet at 1175 Å as a density diagnostic, but it could also be resolved if the UV absorber lies at the base of the ionization cone in the form of clouds. This constituent then represents a transient phase of the gas as it expands, ionizes, and transforms into the much more extended and more tenuous X-ray plasma.

This work is based on observations obtained with *XMM-Newton* an ESA science mission with instruments and contributions directly funded by ESA Member States and the USA (NASA). EB acknowledges helpful discussions on AGN phenomenology with Ari Laor. EB was supported by the Yigal-Alon Fellowship and by the GIF Foundation under grant #2028-1093.7/2001. The MSSL authors acknowledge the support of PPARC. SRON is supported financially by NWO, the Netherlands Organization for Scientific Research. MS was

supported by NASA through *Chandra* Postdoctoral Fellowship Award Number PF1-20016 issued by the *Chandra* X-ray Observatory Center, which is operated by the Smithsonian Astrophysical Observatory for and on behalf of NASA under contract NAS8-39073. We thank an anonymous referee for a thorough and helpful report.

## REFERENCES

Antonucci, R. R. J., & Miller, J. S. 1985, ApJ, 297, 621

Appenzeller, I. & Östreicher, R. 1988, AJ, 95, 45

Appenzeller, I. & Wagner, S. J. 1991, A&A, 250, 57

Bar-Shalom, A., Klapisch, M., & Oreg, J. 2001, J. Quant. Spectr. Radiat. Transfer, 71, 169

Behar, E., Sako, M., & Kahn, S. M. 2001 ApJ, 563, 497

Behar, E., Kinkhabwala, A., Sako, M., Paerels, F., Kahn, S. M., Brinkman, A. C., Kaastra, J. S., & van der Meer R. 2002, in *Mass Outflows in AGNs: New Perspectives*, eds. D. M. Crenshaw, S. B. Kraemer, & I. M. George. San Francisco, p.43 (astro-ph/0106398)

Behar, E., & Netzer, H. 2002, ApJ, 570, 165

Behar, E. & Kahn, S. M. 2002, in *NASA Laboratory Astrophysics Workshop* (astro-ph/0210280)

Bhatia, A. K. & Kastner, S. O. 1993, ApJ, 408, 744

Blustin, A. J., Branduardi-Raymont, G., Behar, E., Kaastra, J. S., Kahn, S. M., Page, M. J., Sako, M., & Steenbrugge, K. C. 2002, A&A, 392, 453

Blustin, A. J. et al. 2003, A&A, 403, 491

Brinkman, A. C., Kaastra, J. S., van der Meer, R. L. J., Kinkhabwala, A., Behar, E., Kahn, S. M., Paerels, F., & Sako, M. 2002, A&A, 396, 761

Bromage, G. E. et al. 1985, MNRAS, 215, 1

de Vaucouleurs, G., de Vaucouleurs, A., Corwin, H. G., Buta, R. J., Paturel, G., & Fouque, P. 1991, Third Reference Catalogue of Bright Galaxies (NY: Springer)

Gabel, J., et al.2003, ApJ, 583, 178

George, I. M., Turner, T. J., Mushotzky, R., Nandra, K., & Netzer, H. 1998, ApJ, 503, 174

Kaastra, J. S., Steenbrugge, K. C., Raassen, A. J. J., van der Meer, R. L. J., Brinkman, A. C., Liedahl, D. A., Behar, E., & de Rosa, A. 2002, A&A, 386, 427

Kallman, T. & Bautista, M. 2001, ApJS, 133, 221

Kaspi, S., Brandt, W. N., Netzer, H., Sambruna, R., Chartas, G., Garmire, G. P., & Nousek, J. A. 2000, ApJ, 535, L17

Kaspi, S., et al. 2001, ApJ, 554, 216

Kaspi, S., et al. 2002, ApJ, 574, 643

Kinkhabwala, A., et al. 2002, ApJ, 575, 732

Kraemer, S. B., Crenshaw, D. M., & Gabel, J. R. 2001, ApJ, 557, 30

Kriss, G. A., Blustin, A. J., Branduardi-Raymont, G., Green, R. F., Hutchings, J., & Kaiser, M. E., A&A, 403, 473

Krolik, J. H., & Kriss, G. A. 1995, ApJ, 447, 512

Lepson, J. K., Beiersdorfer, P., Behar, E., & Kahn, S. M. 2003, ApJ, 590, 604

Markowitz, A., et al. 2003 ApJ, in press (astro-ph/0303273)

Netzer, H., Chelouche, D., George, I. M., Turner, T. J., Crenshaw, D. M., Kraemer, S. B., & Nandra, K. 2002, ApJ, 571, 256

Ogle, P.M., Brookings, T., Canizares, C.R., Lee, J.C., & Marshall H.L. 2003, A&A, 402, 849

Onken, C. A., & Peterson, B. M. 2002, ApJ, 572, 746

Pounds, K. A., King, A. R., Page, K. L., & O'Brien, P.T. 2003, astro-ph/0305571

Rasmussen, A., Paerels, F., & Kahn, S. M. 2003, in *The IGM/Galaxy Connection: The Distribution of Baryons at z=0*, (astro-ph/0301183)

Sako, M., Kahn, S. M., Paerels, F., & Liedahl, D., ApJ, 543, L115

Sako, M., et al. 2001, A&A, 365, L168

Shields, J. C., & Hamann, F. 1997, ApJ, 481, 752

Steenbrugge, K.C., Kaastra, J.S., de Vries, C.P. & Edelson, R. 2003, A&A, 402, 477

Turner, T. J., Nandra, K., George, I. M., Fabian, A. C., & Pounds, K. A. 1993, ApJ, 419, 127

Young, A. J., Wilson, A. S., & Shopbell, P. L. 2001, ApJ, 556, 6

Table 1. Ions seen in absorption in the RGS spectrum of NGC 3783.

| Ion | Outflow Velocity [km s$^{-1}$] | $v_{turb}$ [km s$^{-1}$] [a] | $N_i$ [$10^{18}$ cm$^{-2}$] |
|---|---|---|---|
| O VIII | $-550 \pm 230$ | $170 \pm 50$ | $4.0 \pm 1.0$ |
| O VII | $-660 \pm 230$ | $170 \pm 50$ | $1.0 \pm 0.3$ |
| O VI | $-800 \pm 230$ | $170 \pm 50$ | $0.01 \pm 0.01$ |
| O V | $-470 \pm 230$ | $170 \pm 50$ | $0.18 \pm 0.03$ |
| O IV | $-770 \pm 230$ | $170 \pm 50$ | $0.08 \pm 0.02$ |
| O III | — | — | $\leq 0.005$ |
| O II [b] | $\pm 230$ | $kT_i$=0.1 eV [c] | $0.004 \pm 0.01$ |
| O I [d] | $\pm 230$ | $kT_i$=0.02 eV | $0.025 \pm 0.035$ |
| O VII Gal. [e] | z = $0.0018 \pm 0.0008$ | 40; $kT_i$=0.1 keV | $0.084 \pm 0.03$ |

[a] Turbulent velocities of O IV - O VIII were tied together in the fit.

[b] Blended with O I in our galaxy.

[c] Ion temperature.

[d] Blended with Ar XVI in NGC 3783.

[e] Tentative identification.

Table 2. Oxygen emission lines in the RGS spectrum of NGC 3783.

| Ion | Observed Wavelength [Å] | Velocity Shift [km $s^{-1}$] [a] | Velocity Width [km $s^{-1}$] [b] | Line Flux [$10^{-5}$ cts $s^{-1}$ $cm^{-2}$] | Line Flux [$10^{-5}$ cts $s^{-1}$ $cm^{-2}$] (Kaspi et al. 2002) |
|---|---|---|---|---|---|
| O VIII Ly$\alpha$ | 19.173 | 330 ± 230 | 740 ± 140 | 4.5 ± 0.8 | 2.32 ± 0.74 |
| O VII $r$ | 21.833 | 290 ± 230 | 740 ± 140 | 7.8 ± 1.5 | 4.58 ± 2.38 |
| O VII $i$ | 22.034 | 290 ± 230 | 740 ± 140 | 4.1 ± 1.3 | 3.52 ± 1.82 |
| O VII $f$ | 22.335 | 290 ± 230 | 740 ± 140 | 11.5 ± 1.6 | 10.13 ± 2.74 |

[a] In the system of NGC 3783 and tied for all O VII lines.

[b] Tied for all lines.

Table 3. Measured and derived parameters for the X-ray emitter/absorber in NGC 3783 as traced by O VII & O VIII.

| Parameter | O VII ($f$) | O VIII (Ly$\alpha$) | UV (Gabel et al. 2003) |
|---|---|---|---|
| $\xi$ [erg s$^{-1}$ cm] | 30 | 30 | |
| $L$ [$10^{43}$ erg s$^{-1}$] | 1.5 | 1.5 | |
| $N_i$ [$10^{18}$ cm$^{-2}$] | 1.0 ± 0.3 | 4.0 ± 1.0 | |
| $f_q$ | 0.14 | 0.57 | |
| $f_{q+1}$ | 0.57 | 0.29 | |
| $A_O$ | $5\times10^{-4}$ | $5\times10^{-4}$ | |
| $N_H$ [$10^{22}$ cm$^{-2}$] | 1.43 ± 0.43 | 1.40 ± 0.35 | |
| $d$ [Mpc] | 41.8 | 41.8 | |
| $F_{ji}$ [$10^{-5}$ cts s$^{-1}$ cm$^{-2}$] | 11.5 ± 1.6 | 4.5 ± 0.8 | |
| $P_{ji}$ [$10^{-12}$ s$^{-1}$ cm$^3$] | 3.9 | 5.7 | |
| $EM$ [$10^{64}$ cm$^{-3}$] | 2.2 ± 0.3 | 1.2 ± 0.3 | |
| Localized Clouds Scenario ($r_{max} - r_{min} = \Delta r \ll r$) | | | |
| $r$ [pc] | 16.3 ± 7.3 | 12.3 ± 4.9 | $\lesssim 0.26$ |
| $\Delta r$ [pc] | 9.9 ± 3.0 | 8.1 ± 2.1 | $3.3\times10^{-9}$ |
| $n_e$ [cm$^{-3}$] | 200 ± 180 | 340 ± 270 | $10^9$ |
| $v_{out}$ [km s$^{-1}$] | −600 ± 150 | −600 ± 150 | −550 - −1300 |
| $M$ [$10^{37}$ g] | 1.0 ± 1.3 | 1.0 ± 1.1 | $1.8\times10^{-22}$ |
| $\dot{M}$ [$10^{33}$ g yr$^{-1}$] | 0.6 ± 0.7 | 0.8 ± 0.8 | $3.4\times10^{-13}$ |
| $\Omega \cong (\Delta r/r)^2$ [str] | — | — | $1.6\times10^{-16}$ |
| Ionization Cones Scenario ($r_{max} \gg r_{min}$) | | | |
| $r_{min}$ [pc] | 9.4 ± 2.8 | 9.6 ± 2.4 | $\lesssim 0.26$ |
| $n_e(r_{min})$ [cm$^{-3}$] | 590 ± 350 | 560 ± 280 | $10^9$ |
| $\Omega/2\pi$ | 0.24 ± 0.08 | 0.13 ± 0.05 | $2.6\times10^{-17}$ |
| $v_{out}$ [km s$^{-1}$] | −600 ± 150 | −600 ± 150 | −550 - −1300 |
| $M/r_{max}$ [$10^{36}$ g pc$^{-1}$] | 8.4 ± 2.6 | 4.7 ± 1.8 | $M = 1.8\times10^{15}$ g |
| $\dot{M}$ [$10^{33}$ g yr$^{-1}$] | 5.2 ± 2.0 | 2.7 ± 1.0 | $3.4\times10^{-13}$ |

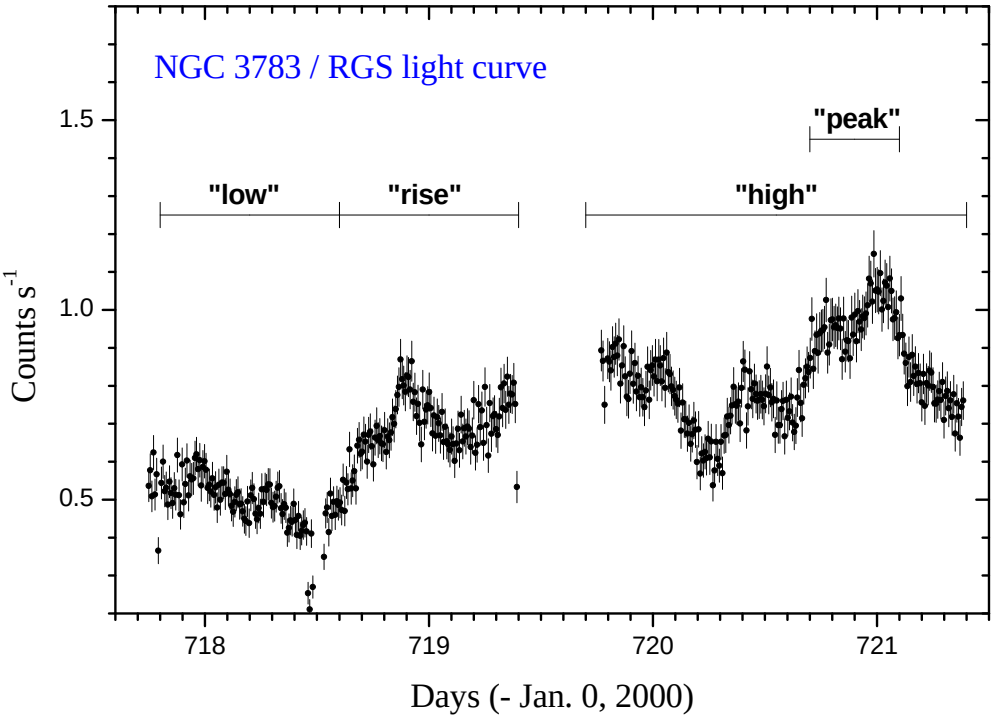


Fig. 1.— The RGS light curve (RGS 1 and 2 combined) during the present 280 ks observation in time bins of approximately 10 minutes. Different segments of the observations have been labeled.

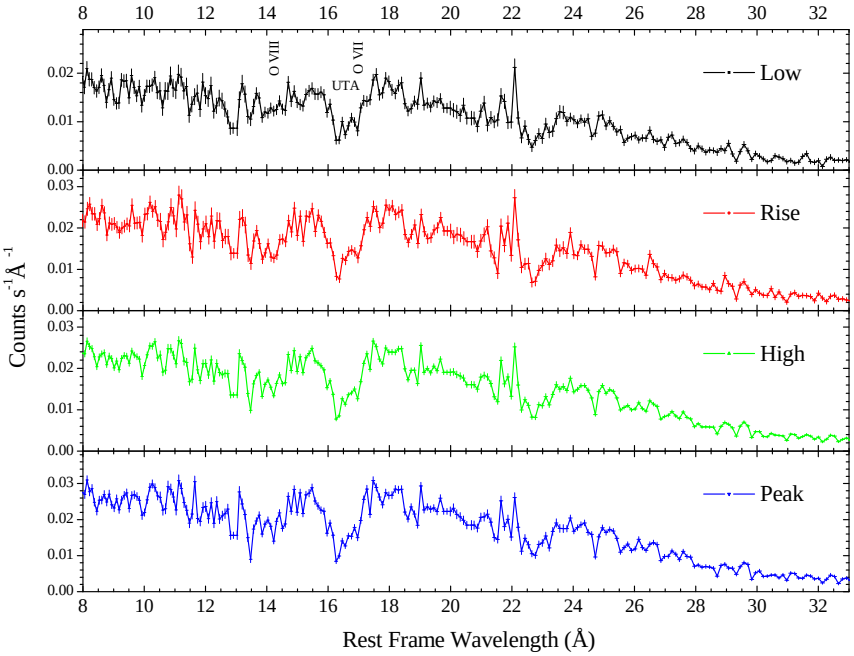


Fig. 2.— The RGS spectra during the four time segments defined in Fig. 1. The data are plotted in bins of about 0.1 Å to accentuate broad structure. Hence also the small error bars. The lines between the data points are plotted just to guide the eye. Apart from the different flux levels, the shape of the absorption structure appears to be remarkably similar in all four spectra. In particular, the broad absorption features due to the Fe-M 2p-3d UTA (16 -17 Å) and due to the O-K edges (14.2 & 16.8 Å) do not appear to vary. The quality of the data is not good enough to enable detection of variability in the narrow lines.

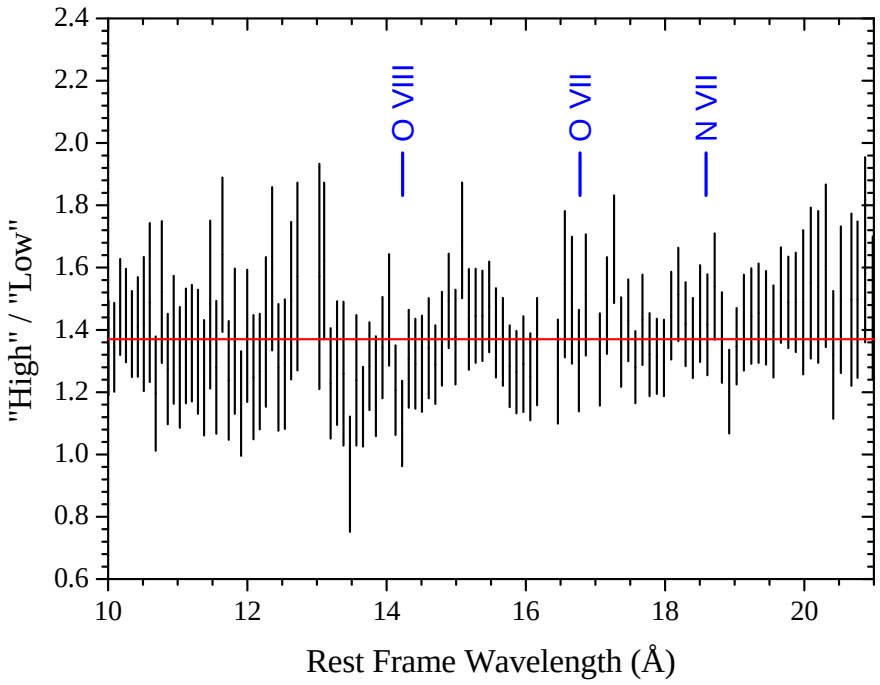


Fig. 3.— Ratio of the "high" phase and "low" phase spectra rebinned to about 0.1 Å. No appreciable broad deviations from the mean (horizontal line) are found implying no significant change in the photoelectric edges (marked above the data). The gaps in the plot are instrumental. Note that even with no change in absorption, the ratio around strong emission and absorption lines (e.g., at 13.5, 14.2, 15, and 19 Å) is not expected to be perfectly flat, since deep absorption troughs suffer from low S/N and emission lines do not cancel out in the ratio.

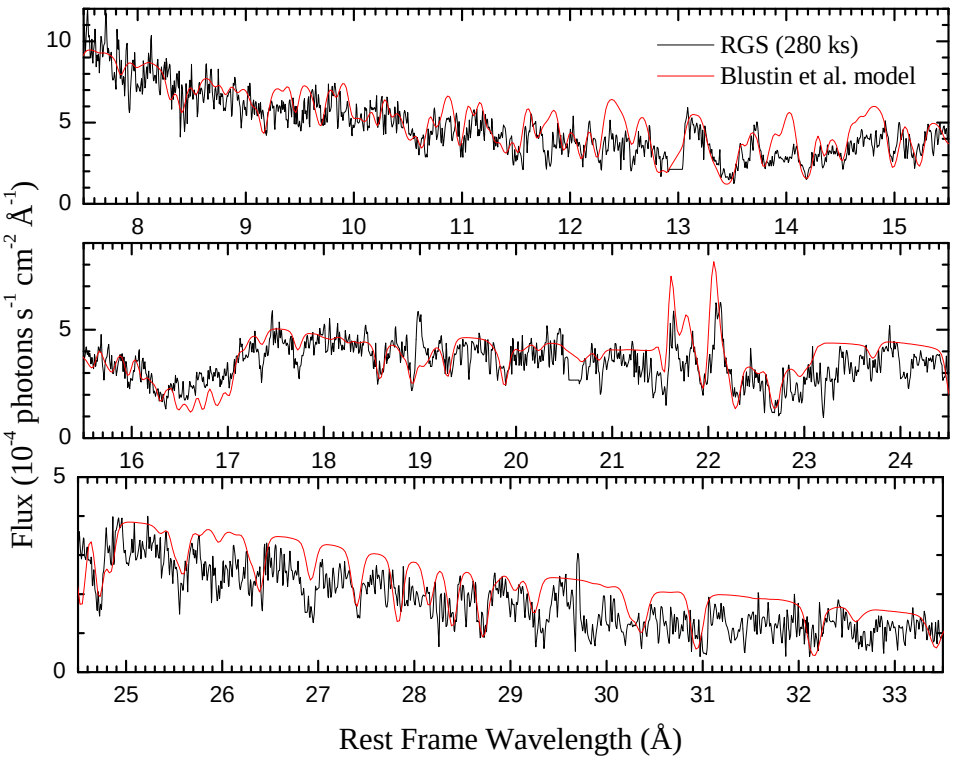


Fig. 4.— The total 280 ks RGS spectrum of NGC 3783. The slab model from Blustin et al. (2002), which was fitted to the first 40 ks RGS observation, is over-plotted with no adjustments, including no re-normalization. The over all agreement is very good, but noticeable discrepancies are seen in the details of the O-K region between 14 and 24 Å.

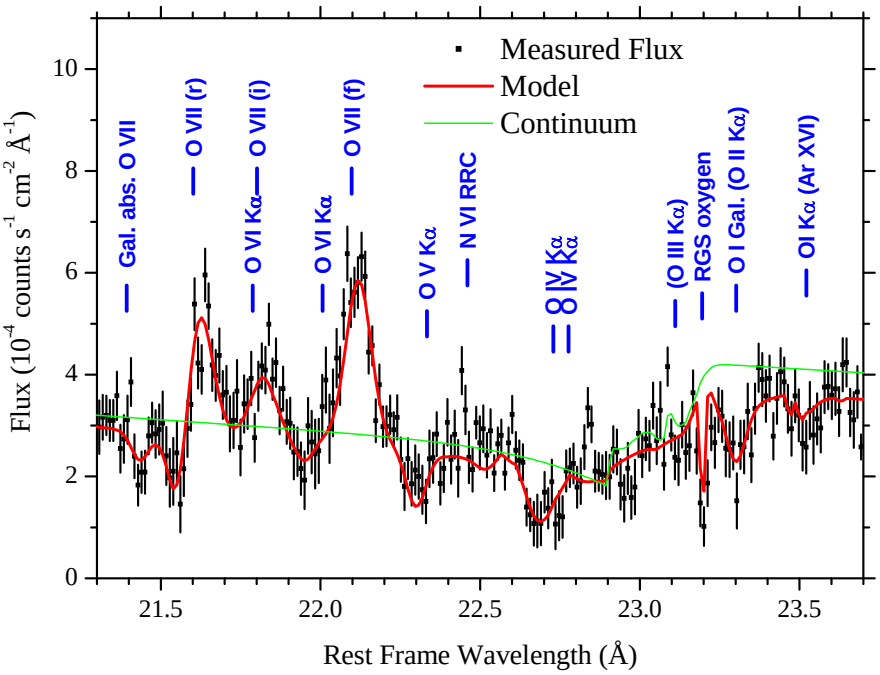


Fig. 5.— Spectrum of NGC 3783 in the region of the K$\alpha$ lines of O I - O VII as obtained with a 280 ks RGS observation. The thick curve represents the best-fit model and the thin curve is the continuum model only with galactic and instrumental absorption.

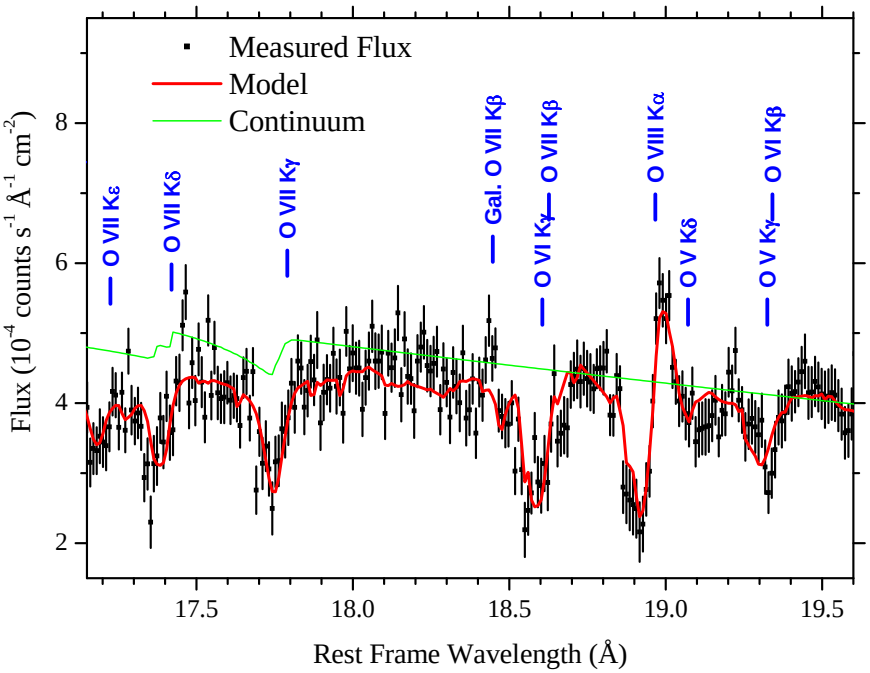


Fig. 6.— Spectrum of NGC 3783 showing the region of O VIII K$\alpha$ as well as higher order lines (K$\beta$, K$\gamma$, etc.) of lower charge states of O as obtained with a 280 ks RGS observation. The thick curve represents the best-fit model and the thin curve is the continuum model only with galactic and instrumental absorption.